Optical turbulence in phase-conjugate resonators

G. Reiner* and M. R. Belić†

Max-Planck-Institut für Quantenoptik, D-8046 Garching, Federal Republic of Germany

P. Meystre

Optical Sciences Center, University of Arizona, Tucson, Arizona 85721

Received September 15, 1987; accepted December 21, 1987

Instabilities and transition to optical turbulence in a phase-conjugate resonator are numerically investigated under the influence of more than one control parameter. The dynamics of intracavity modes, including one transverse spatial dimension, is considered under various conditions and in different regions of the multidimensional parameter space. A great variety of phenomena is observed, including Feigenbaum, intermittency and the Ruelle–Takens–Newhouse route to chaos, spatial filamentation and making the beam profile chaotic, coexisting attractors and boundary crises, optical bistability and dynamical effects, and inverse bifurcations. The route to high-dimensional chaos in this infinitely dimensional dissipative dynamical system is monitored qualitatively and quantitatively by using embedding techniques, Fourier and Lyapunov spectra, Poincaré sections, and bifurcation diagrams. We find similarities and significant differences with other infinite systems, notably with fluid dynamical flows and a time-delay differential equation.

1. INTRODUCTION

The problem of turbulence remains one of the few unresolved old scientific problems. Although significant progress has been made lately toward understanding low-dimensional chaos,[1] owing largely to the advent of fast computational methods and machines (and clever experiments), the fully developed turbulence, so it seems, is waiting for the next generation of supercomputers. In this paper we would like to add to the understanding of the low-dimensional turbulence in an infinitely dimensional system by an analysis, necessarily numerical, of the dynamics of intracavity modes in a phase-conjugate resonator (PCR).[2] Nonlinear-optical systems[3] seem to be especially well suited for such an analysis, as compared, for example, with the fluid Navier–Stokes systems[4] because they can be described in terms of relatively simple models that permit efficient numerical simulation and also are amenable to experimental verification. Furthermore, they exhibit a great variety of interesting dynamical phenomena, as is witnessed in the rapidly developing field of laser instabilities in previous literature[5] and in this special issue and as is presented by this paper.

The system of interest here is a PCR in which the phase-conjugate mirror (PCM) is represented by a nonlinear Kerr-like medium operating in the thin-hologram regime. This system has been considered by us already in a few publications[6–8] and in various degrees of approximation and numerical sophistication. Here, we continue and also summarize our investigations of the dynamical responses of the cavity by presenting a few interesting study cases concerned with the fast and slow response of the medium, filamentation, and spatial chaos of the intracavity field and a well-documented Ruelle–Takens–Newhouse (RTN) transition to chaos through a few bifurcations of a limit cycle. The mode of presentation will be rather descriptive, leaving out mathematical intricacies and numerical details.

Therefore we will not dwell much on the introduction and the theory of the model, as they are amply described in earlier publications.[7,8] The assumed interaction geometry is depicted in Fig. 1, where F_0 and B_0 denote two counterpropagating laser beams pumping the Kerr-type PCM located at $z = 0$. A curved normal mirror with a spatial aperture in front of it is positioned so as to return the first-order scattered light at an angle θ back into the resonator. The size of the aperture is one of the control parameters in the problem, as are the pump intensities. The other control parameters include focusing or defocusing in the Kerr medium, Fresnel number of the resonator, curvature and reflectivity of the normal mirror, and the size of the Fourier filter (i.e., the number of Fourier components used in the numerical calculations). Not all these parameters will be varied in our numerical experiments.

The numerical procedure consists of the following. The paraxial wave equation for the forward- and the backward-propagating field inside the resonator is solved by using a fast-Fourier-transform (FFT) spectral technique. One transverse spatial dimension is specifically included, so that we consider a striped-resonator configuration. We have no reason to believe that inclusion of the other transverse dimension would dramatically change our conclusions. Phase-conjugate reflection off the PCM is achieved by using reflectivity formulas from Ref. 7 and by solving the diffusion equation for the phase shift accumulated in a PCM by using

0740-3224/88/051193-18$02.00

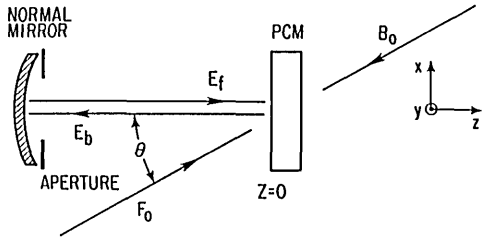

Fig. 1. Geometry of four-wave mixing PCR used in our simulations. It permits first-order scattered PC light at an angle θ to be reflected back into the resonator.

a fourth-order Runge–Kutta method. Thus the transverse coupling is provided by diffraction in the cavity and by diffusion in the Kerr medium. Depending on the case studied, the diffusion is sometimes set to zero (fast media), and sometimes no explicit reflectivity formula is used (slow media). The programs are run on a vectorized multiprocessor machine. The full description of our numerical scheme, again, can be found in Refs. 7 and 8.

An indication of the complexity and richness of the phenomena in the general case is revealed by considering a simplified plane-wave two-dimensional-map approximation

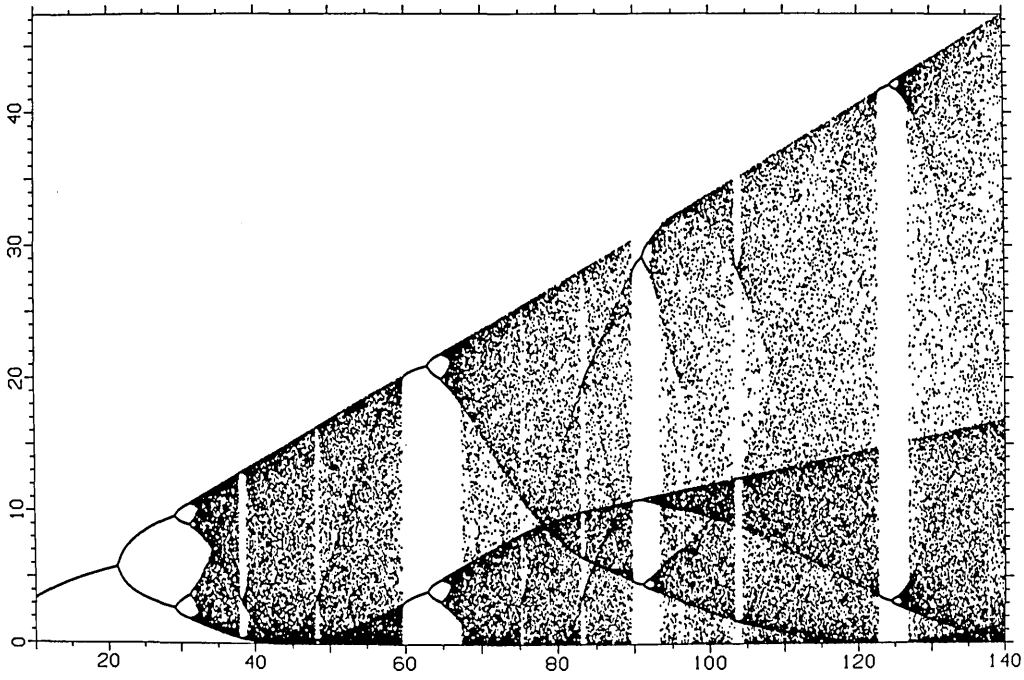

Fig. 2. Bifurcation diagram of a one-dimensional PCR plane-wave model represented by a first-order Bessel function map, Eq. (1). The driving parameter A is proportional to the pump intensity.

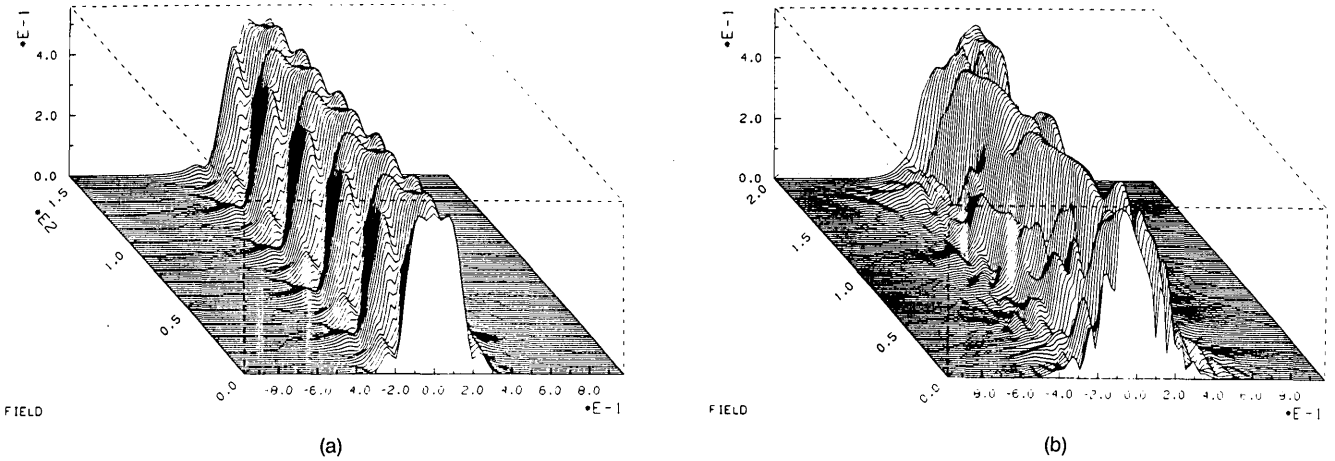

Fig. 3. A (a) periodic and a (b) chaotic response of the phase-conjugate cavity under an increasing number of spatial Fourier components. The transverse profile of the phase-conjugate field $|E_b|$ (see Fig. 1) is shown at different times. The displayed time intervals amounted to 150 medium response times in (a) and 200 in (b). The time scale is displaced in both cases, i.e., initial transient intervals are not shown. The pump intensity equals $I_p = 1.2$ in units of the threshold oscillation intensity, and the threshold (initial) signal E_f is Gaussian. It slowly gets deformed as the pump intensity is increased from 1. to 1.2, more rapidly so for case (b).

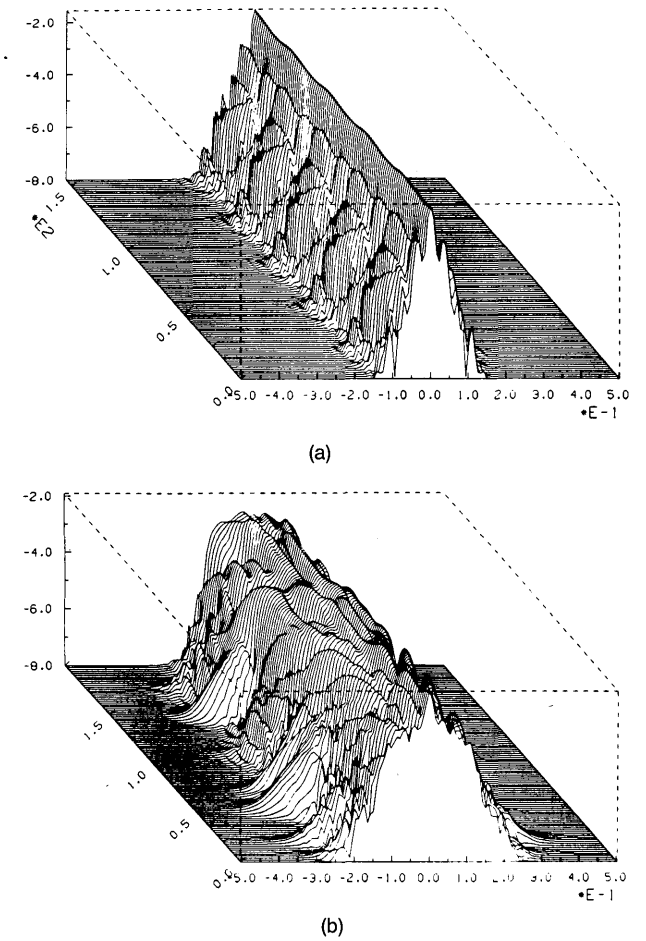

Fig. 4. Spatial spectral decomposition of the beam profiles from Fig. 3, obtained by a FFT algorithm.

to the problem, as presented in Ref. 6. It was discovered in Ref. 6 that the intracavity intensity after consecutive round trips obeys a map relation

$$x_{n+1} = A J_1^2(x_n)^{1/2}, \tag{1}$$

and the phase executes a quasi-periodic distance-preserving hopping. Here $x_n = 4|F_0E_n|^2$, $A = 4\rho|F_0B_0|^2$ is the pump-driving parameter, ρ is the normal mirror reflectivity, and J_1 is the first-order Bessel function. The dimensionless intensities are measured in units of $c/\omega n_2 d$, where d is the medium thickness. It is seen that when the pump intensity is increased to a certain value of A, the intracavity field becomes unstable. When the intensity undergoes a period doubling, the phase becomes indeterminate but not chaotic: the Lyapunov exponent of the phase evolution always remains zero. The dynamical behavior of the intensity, on the other hand, is complex, owing to the complex form of the mapping function. Its bifurcation diagram is represented in Fig. 2 as a function of the pump parameter. It is seen that for low pump intensity the transition to chaos follows a Feigenbaum scenario, coming from the inverted-parabola look of the first lobe of the Bessel function. As the pump intensity increases, the higher lobes of the J_1 function come into play, and the bifurcation diagram past the accumulation point loses any resemblence to the Feigenbaum scenario. However, its global, topological outlook is amenable to an analysis

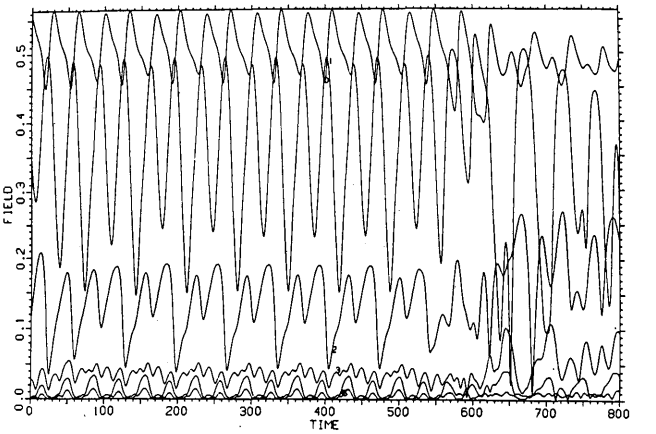

Fig. 5. Temporal sequences of the points at various transverse locations, from the tip of the beam, $x = 0$, to $x = 0.5$ in the wings (in units of the backward pump beam waist). The case presented is between (a) and (b) from Fig. 3, showing intermittent chaotic bursts. It is interesting to note that points at different transverse locations execute different periodic motions, but they all go chaotic simultaneously, indicating strong transverse correlations.

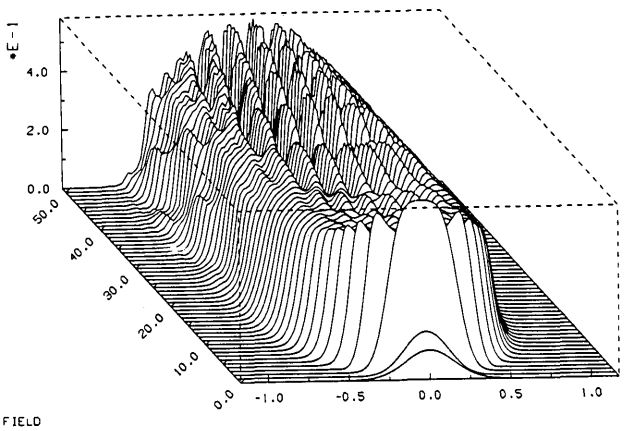

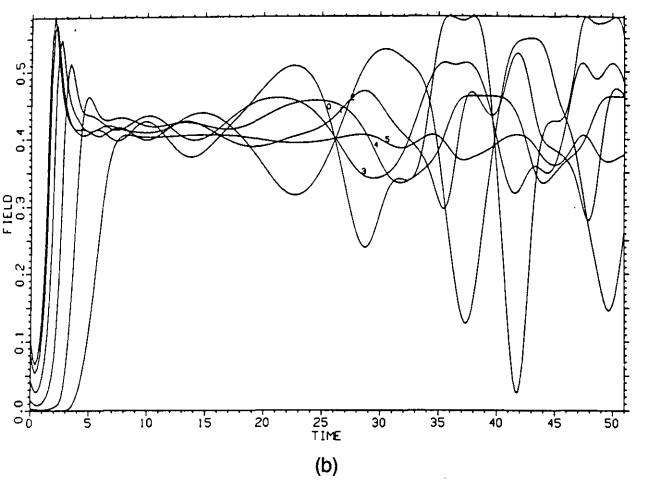

Fig. 6. (a) Transverse beam filamentation in the case of a defocusing medium and in a low diffraction geometry. The pump intensity is $I_p = 3.5$, and the first 50 medium response times are followed. The initial rapid switchup with an overshoot is distinctly visible. (b) Behavior at different transverse locations is definitely irregular, even though a coherent fairly stable spatial structure evolves.

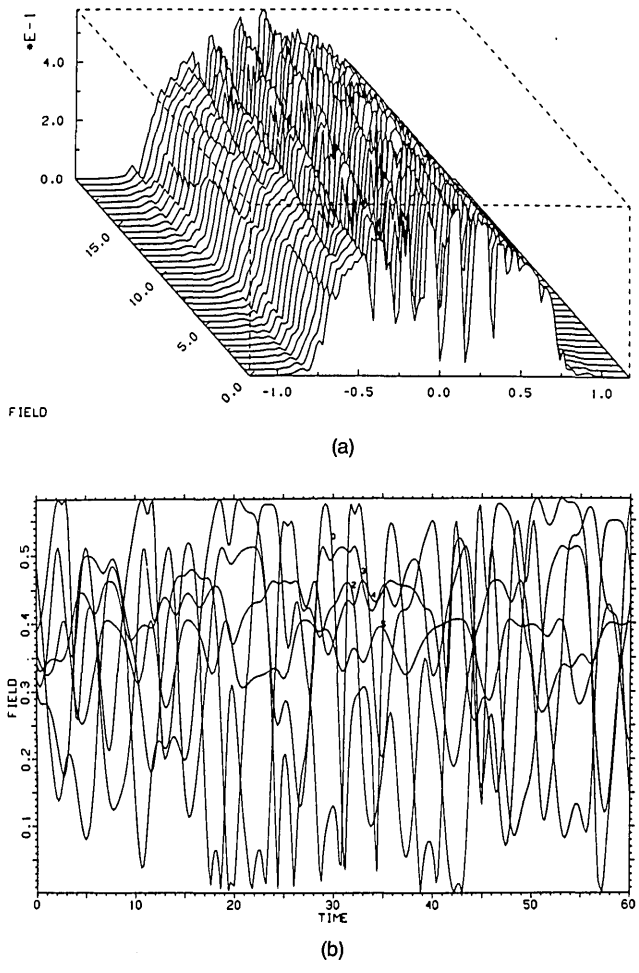

Fig. 7. Same as Fig. 6 but for a higher pump intensity, $I_p = 4.2$, and after the first 50 MRT have expired.

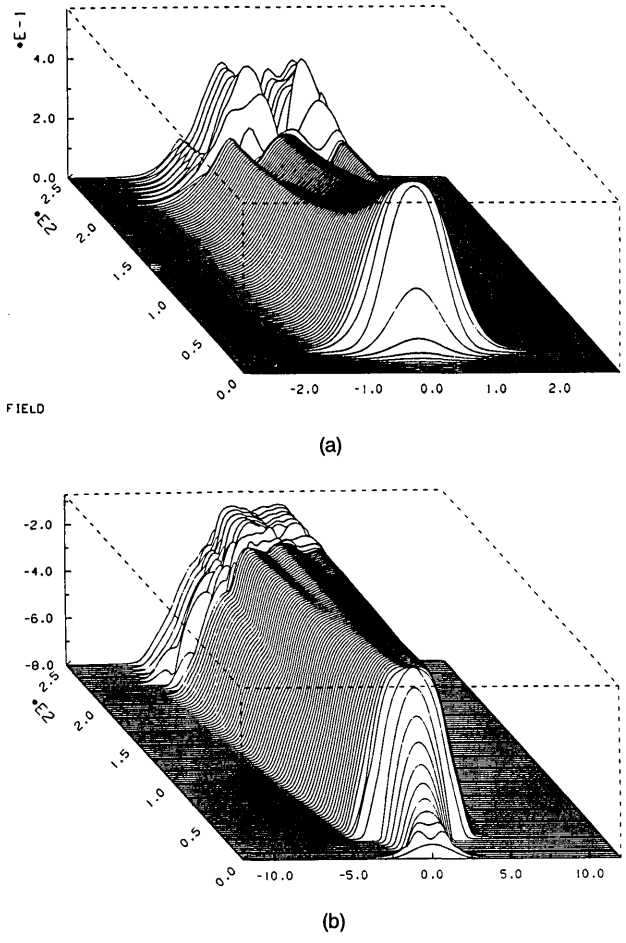

Fig. 8. Phase-conjugate beam development for the focusing medium and a high diffraction geometry: (a) depicts the transverse profiles and (b) shows the corresponding spatial Fourier transforms. The region 1–9 in pump intensity is swept up in 250 steps to pinpoint the occurrence of instabilities. The field development is seen to proceed gradually and symmetrically until $I_p \simeq 7.5$, when the instability breaks in.

by symbolic dynamical[9] methods. For example, equations for the dark accumulation lines running through chaotic regions or positions of the periodic windows and their structure are readily found by using symbolic methods. Such an analysis is performed along the following lines.

The mapping of Eq. (1) in terms of a Bessel function has a set of zeros and a set of maxima located between the zeros. Collectively, these points are denoted as the critical points $\{x_c^i\}$ of the map. Suppose that in the beginning the input values for x_n are uniformly distributed and that we are inside a chaotic region. After just one iteration the new x_{n+1} values will become nonuniform, clustered around the images of the critical points. Two of these images also define the extrema of the map, i.e., the boundaries of the output. After many iterations it is clear that the images of the critical points will define a set of maxima in the distribution of x, which will show up in the bifurcation diagram as locations of the accumulation lines inside the chaotic region. Therefore for each of the critical points a set of polynomials can be defined:

$$P_0^i(A) = x_c^i, \tag{2a}$$

$$P_{n+1}^i(A) = AJ_1^2[P_n^i(A)]^{1/2}. \tag{2b}$$

These polynomials, when plotted as functions of A, deter-

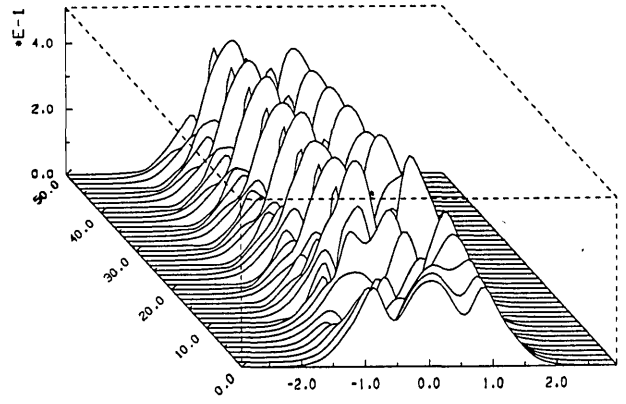

Fig. 9. Temporal establishment of the asymmetric dancing mode at $I_p = 7.5$.

mine locations of the dark lines embedded in a chaotic region. For example, all the polynomials for the first zero (which is not exactly a critical point but behaves like one) equal zero, and the zero line defines the lower boundary of the bifurcation diagram. In contrast, the upper boundary is determined by the first polynomial $P_1^1 = AJ_1^2(x_c^1)^{1/2}$ of the first, largest maximum of the J_1 function. All straight lines

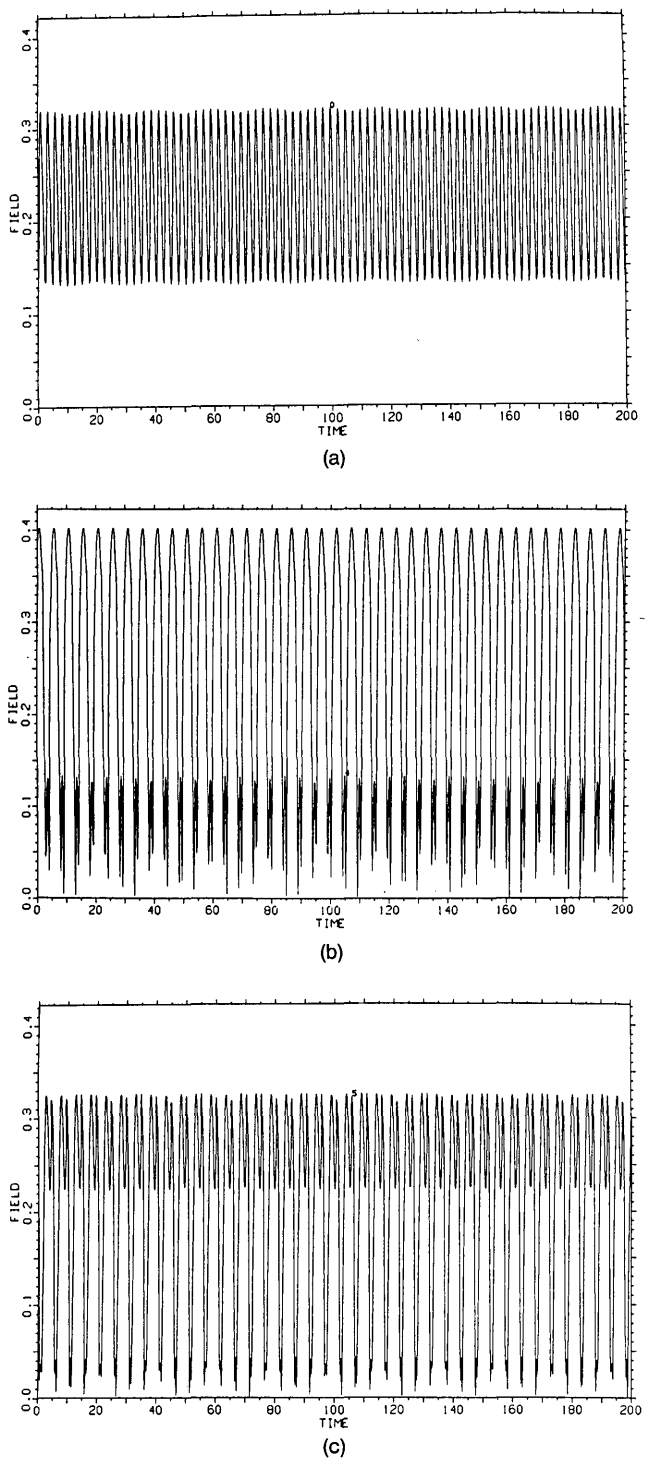

Fig. 10. Periodic oscillations at different transverse locations of the phase-conjugate beam: (a) period 2 at the peak of the beam, (b) period 4 at $x = 0.45$, and (c) period 6 at $x = 0.6$. Period 2 oscillates at double the frequency. Longer-period subharmonics are also present.

seen in the diagram actually come from the first-order polynomials of different critical points. Further, locations of the superstable n orbits (around which periodic windows form in chaotic regions) are found among the real roots of the equations $P_n(A) = x_c$ for arbitrary i. The details of the symbolic analysis of the map [Eq. (1)] will be presented elsewhere.

This paper deals with the overall response of a PCR, including transverse effects, in a numerical setup that closely resembles experimental situation and that cannot be accessed or explained by a plane-wave analysis. The rest of the paper is organized as follows. In Section 2 dynamical solutions for the slow medium and associated transverse effects are considered. In particular, a case of a high-diffraction dancing mode and a low-diffraction filamentation is presented. In Section 3 fast-medium responses are discussed, including a case of a RTN scenario and interesting inverse bifurcations occurring in strange-looking windows in high-dimensional chaos. Section 4 is reserved for conclusions.

2. SLOW MEDIUM

In this section we investigate the dynamical behavior of the PCR in the limit when the medium response time (MRT) is much longer than the cavity round-trip time. To reduce the dimension of the parameter space, we consider only a plane, perfectly reflecting normal mirror with no aperture in front of it, and we assume that the medium is lossless. In actual simulations, in addition to the pump intensity, we vary the Fresnel number F_r (high/low diffraction), the n_2 Kerr coefficient (focusing/defocusing medium), the spatial extent of the pumps (plane/Gaussian), and the size of the spatial Fourier frequency filter (number of Fourier components). Of course, not all parameters will be varied here, nor will all the possibilities be presented.

An overall description of the dynamical response of the cavity is provided in Ref. 7. A typical case is presented in Figs. 3–5, in which periodic and chaotic transverse beam profiles are shown for a low-diffraction ($F_r = 100$) case with a focusing medium, one plane and one Gaussian pump, and above the self-oscillation threshold of the PCR. Figure 3 depicts the temporal evolution (over a few hundred MRT's) of the beam profile for the pump intensity $I_p = 1.2$ (in units of the threshold intensity) when the width of the Gaussian spatial frequency filter is varied. The filter, located in front of the PCM, is introduced to reduce the influence of higher-order spatial modes. In essence, it controls the number of Fourier components used in the decomposition of the waves. The level of truncation is found to influence the intracavity dynamics strongly. Although we observe periodic changes in the intracavity beam profile in Fig. 3(a) (with a period of approximately 30 MRT's for the most pronounced harmonics), the periodicity and the left–right transverse symmetry of the beam is gone in Fig. 3(b), as the frequency window is increased. Figure 4 shows the spatial Fourier spectrum of the profiles from Fig. 3. Evidently, spatial chaotization of the beam produces a widening in the spectral outlook of the mode. More interestingly, in Fig. 5 we see that points at different transverse locations of the beam execute different periodic motions. This is seen even more clearly in the case of high diffraction. However, when there is a sudden change in the dynamics, which is due, for example, to an intermit-

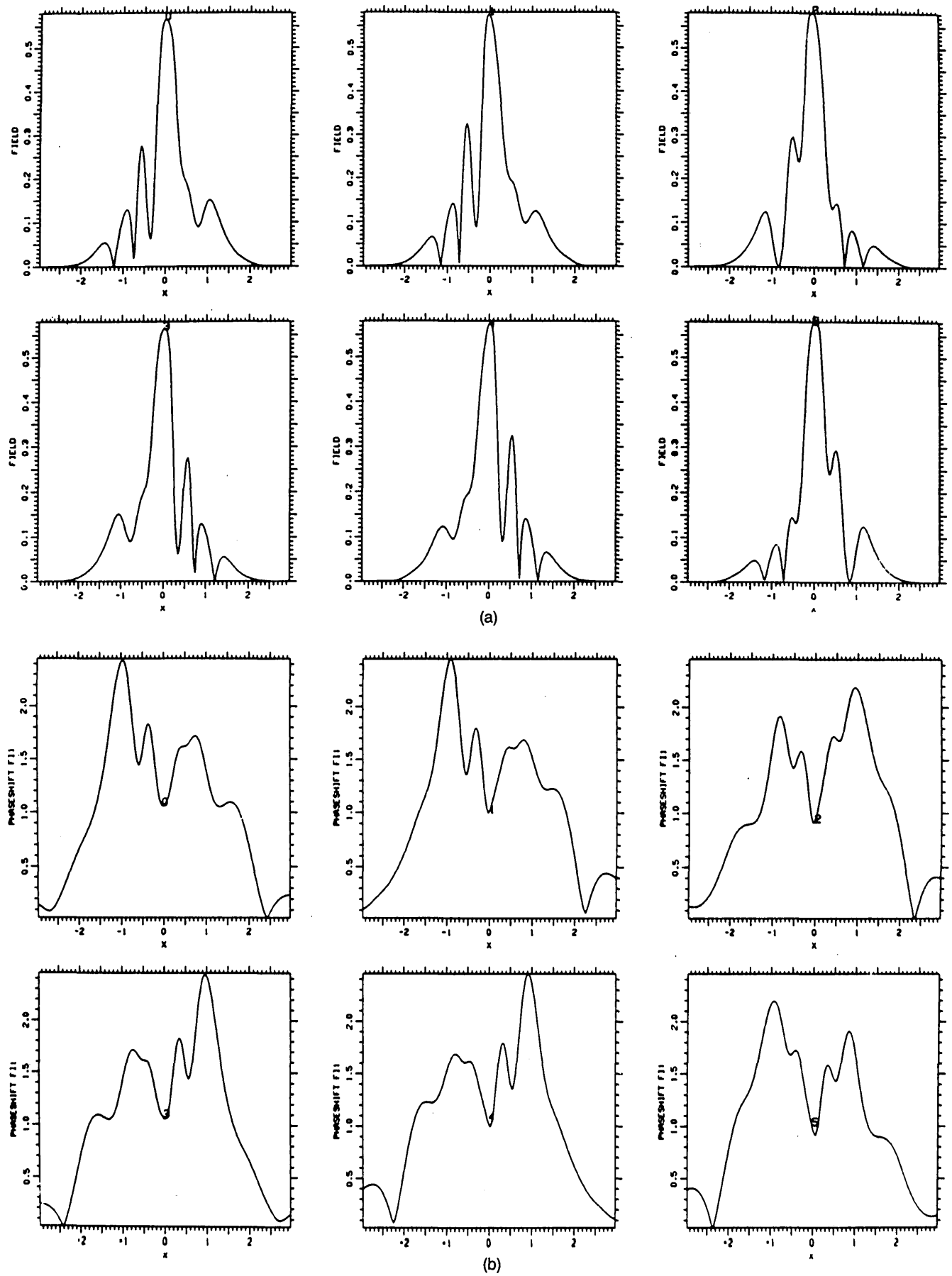

Fig. 11. (a) Field distribution and (b) the phase of the dancing transverse mode. Every 3 MRT's the profile gets inverted about $x = 0$, repeating itself after 6 MRT's.

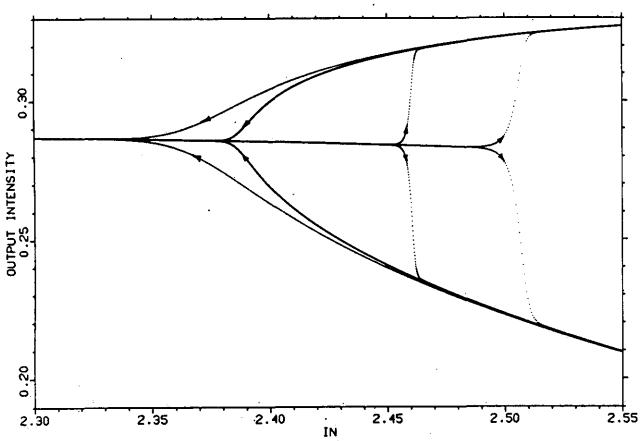

Fig. 12. Dynamical hysteresis loops caused by variable sweep rates across the first bifurcation of the system in Fig. 12. Two up and down sweeps are performed. The large hysteresis loop is obtained when the sweep rate equals $\Delta I_p = 1.25 \times 10^{-4}$, and the smaller one is obtained when $\Delta I_p = 3.125 \times 10^{-5}$. For the sweep rate 10^{-7}, the hysteresis is barely visible.

tent chaotic burst or to a transient or terminal chaos, all transverse points start to execute the new motion simultaneously.

In the case of a defocusing medium in a low-diffraction geometry, with Gaussian pumps and without frequency filtering, the axial Gaussian-like mode at the pump frequency is found to survive up to $I_p \simeq 3.3$. A further increase in I_p results in the development of side-mode instabilities, which eventually cause strong filamentation of the transverse beam profile. A fairly stable, slowly expanding spiky transverse structure results, reminiscent of Moloney's[10] solitons but actually representing a stripe mode in two transverse dimensions. Such a mode would most likely become unstable if the other transverse dimension were included in our calculations. An example of the beam filamentation is shown in Fig. 6, together with the behavior at different spatial points across the beam. The periodic oscillatory motion is seen to cease quickly, and irregular motion sets in. The same effect is more pronounced at a higher pump intensity (Fig. 7), where, although a quasi-stable spatial structure exists (with occasional chaotic bursts in different fingers),

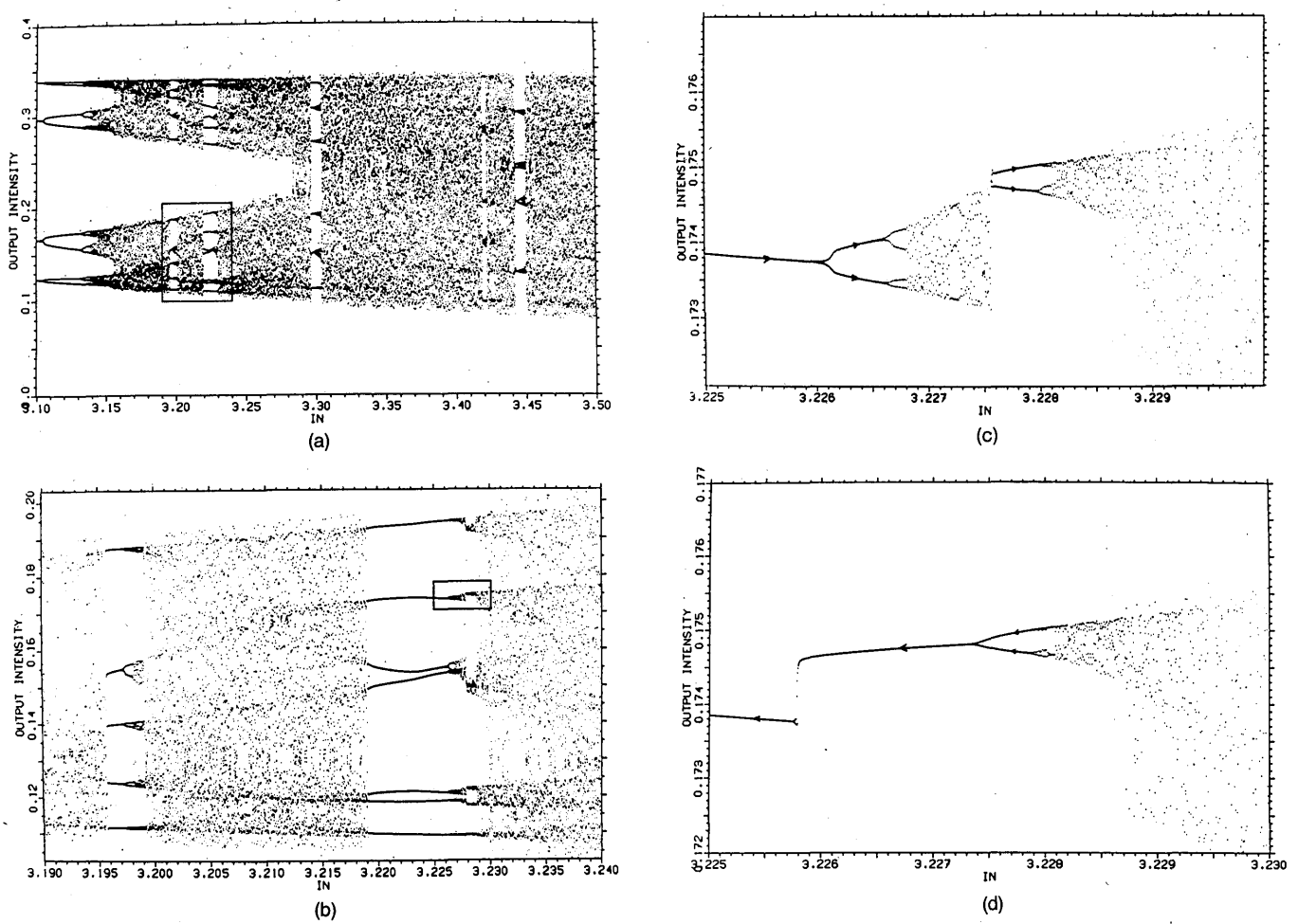

Fig. 13. (a) Bifurcation diagram past the period 4 of the forward-integrated intracavity intensity $I_f = \int dx |E_f(x)|^2$ as a function of the pump intensity I_p. The resonator configuration is nearly confocal, $L/R = 0.9$. The sweep rate is $\Delta I_p = 10^{-5}$. Although it starts as a Feigenbaum, after the accumulation point the diagram barely resembles the period-doubling scenario. (b) The enlarged marked section around period 10 and period 14 windows from (a). In window 14 a sudden change in the attracting set is clearly visible. The marked area is zoomed and swept up in (c) and down in (d). The sweep rate for both up and down sweeps equals 2×10^{-7}.

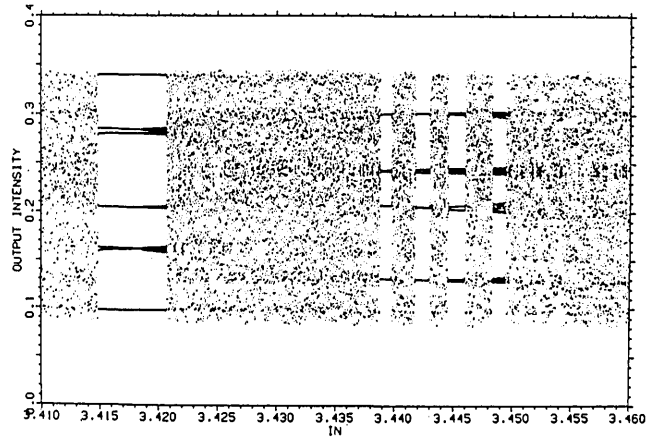

Fig. 14. Suspicious-looking period 7 and 5 windows at $I_p \simeq 3.45$ from Fig. 13(a). On reducing the sweep rate, the period 5 window breaks into intermittent chaos.

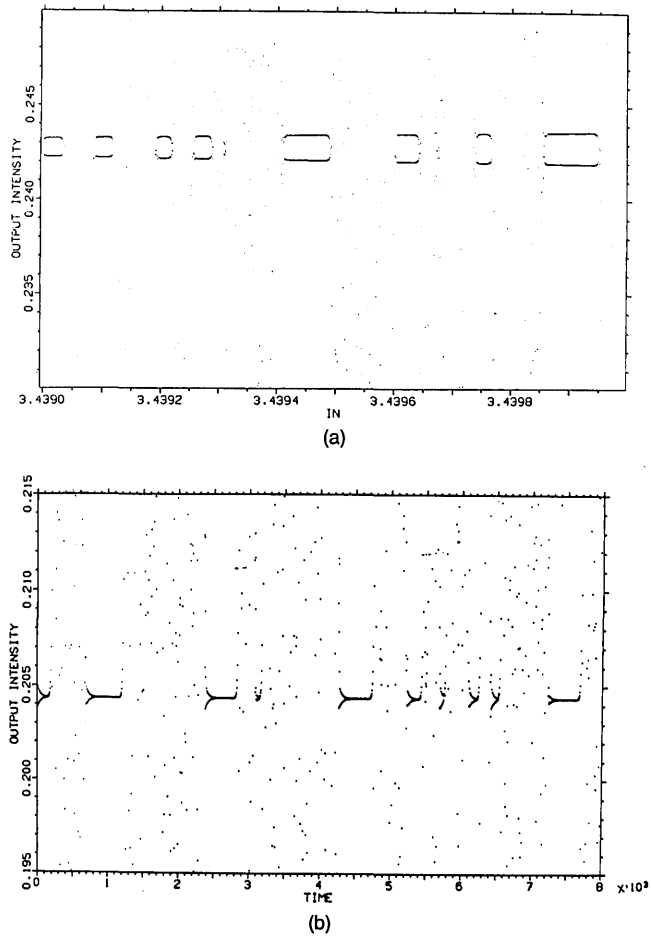

Fig. 15. (a) Very slow (10^{-7}) sweep across the doublet branch in the period 5 window and (b) intermittent time series of the adjacent branch in the same window ($I_p = 3.442$). Qualitatively they look similar. The sweeping nature of the figure (a) can be inferred from the slightly nonparallel arms in the doublet.

various transverse sections of the beam produce apparently chaotic temporal signals.

As a final example we consider a slowly focusing medium in a high-diffraction geometry ($F_r = 1$). The forward pump F_0 is chosen plane, and the backward pump B_0 is a Gaussian focused on the PCM. This configuration is found to lower the threshold for instabilities. The resonator starts to oscillate slightly above $I_p = 1$, and in Fig. 8 the dynamical behavior of the mode is traced in the pump intensity range 1–9. It is seen that the cavity response is gradual and symmetric in the transverse direction, the side modes developing slowly, and the spectrum becoming broader. However, at approximately $I_p \simeq 7.5$ the instability sets in, and there is an abrupt change in the mode outlook. An asymmetric mode develops, whose temporal establishment can be followed in Fig. 9. Its dynamical features are quite striking. First, similar to the low-diffraction focusing case, different spatial points across the beam execute different motions: from a simple period 2 at the center of the beam ($x = 0$) to the period 6 at $x = 0.6$ (in units of the backward pump beam waist). This situation is presented in Fig. 10. The oscillations are now in general more stable than the ones for low diffraction. Moreover, when the temporal development of the mode is followed, we notice that the transverse profile is rhythmically

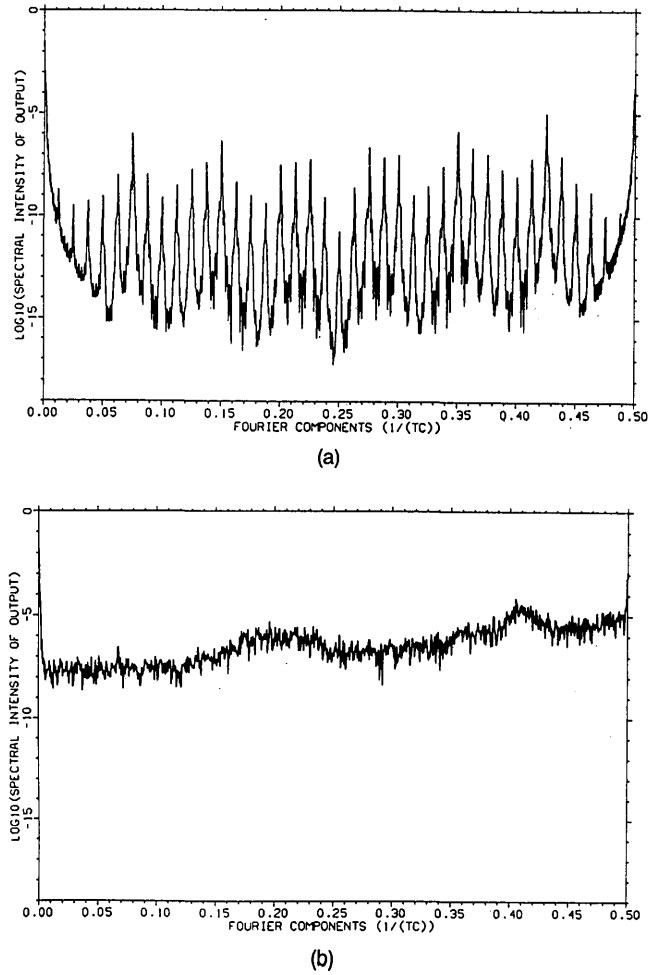

Fig. 16. Fourier spectrum (a) in the periodic window at $I_p = 3.445$ and (b) in the chaotic region at $I_p = 3.49$.

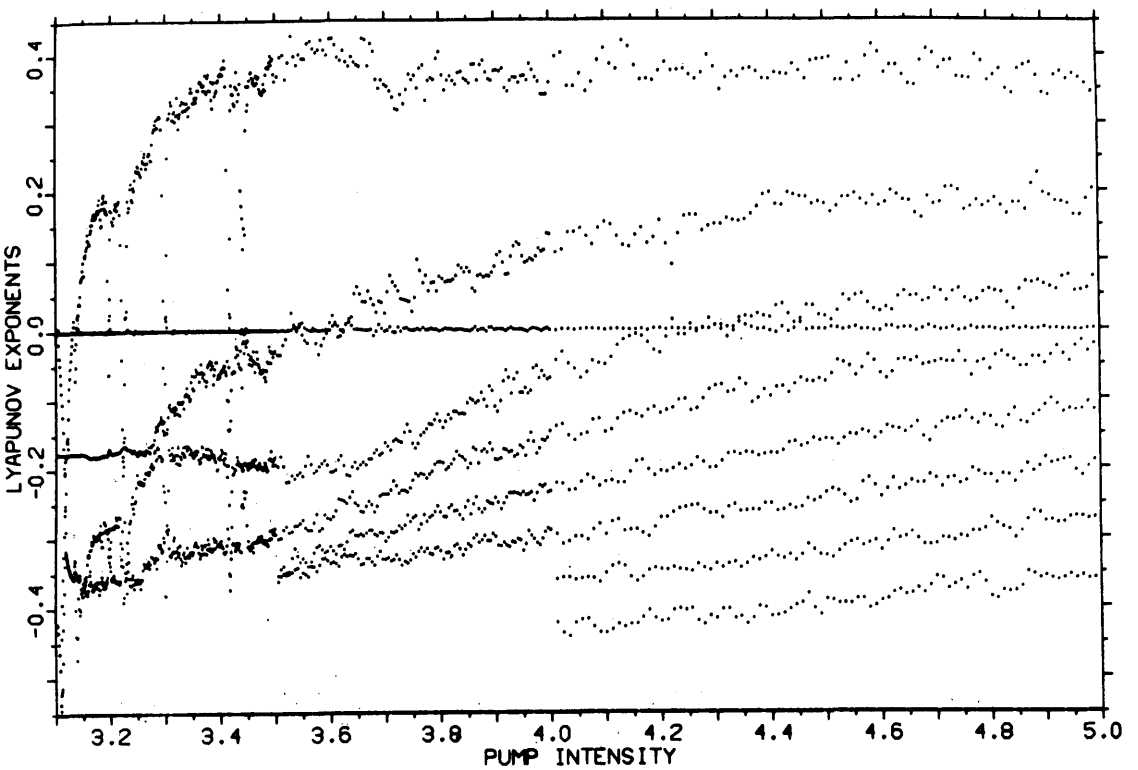

Fig. 17. The spectrum of Lyapunov exponents.

inverted about $x = 0$ every 3 MRT's. The same periodic dance is observed in the phase of the wave (see Fig. 11).

3. FAST MEDIUM

In the case of a fast medium it is assumed that the cavity round-trip time is much longer than the MRT. In this case the problem can be reduced to a return map, which maps intracavity fields after consecutive round trips in the cavity onto each other. Such a description still keeps infinitely dimensional phase space because one transverse dimension is specifically included. However, instead of concentrating on the transverse effects, we will consider the overall response of the cavity by looking at the integrated output intensity at the PCM as a function of the pump-driving intensity. The other relevant parameter will be the size of the aperture placed in front of the normal mirror. Again,

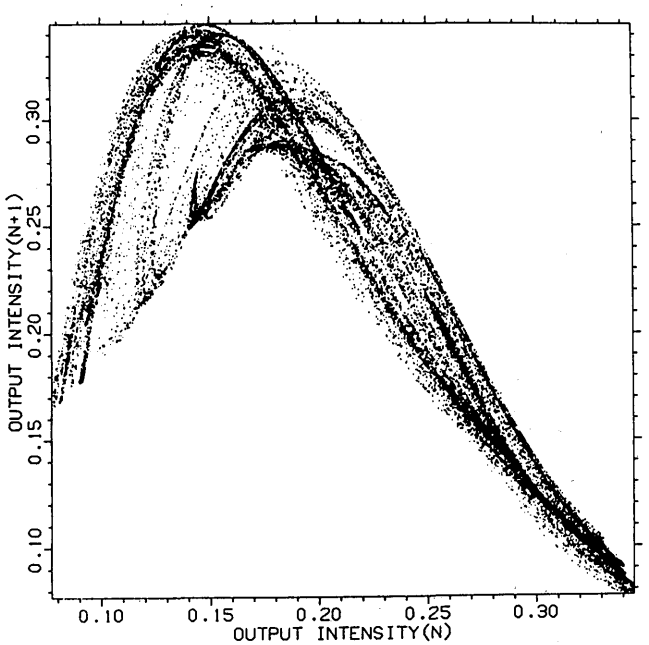

Fig. 18. Poincaré section through the strange attractor at $I_p = 3.5$ with a Lyapunov dimension $D_L \simeq 4.5$.

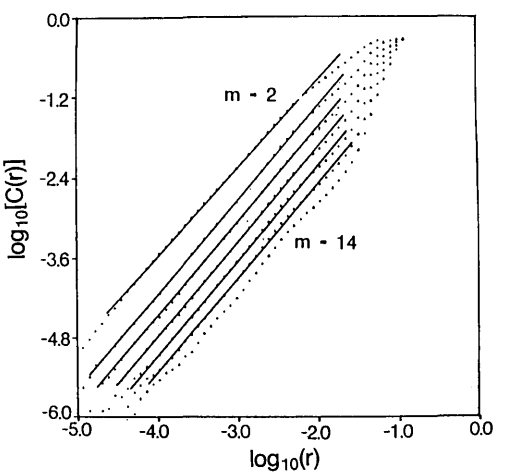

Fig. 19. Calculating the correlation dimension D_2 of the strange attractor at $I_p = 3.18$. The dimension is found from the slope of the $C(r)$ function, which counts the number of pairs of points on the attractor whose distance is less than r. The attractor is embedded in $m = 2, 4, \ldots, 14$ dimensional Euclidian space, and the correlation dimension of the attractor is found to be $D_2 = 2.435 \pm 0.015$.

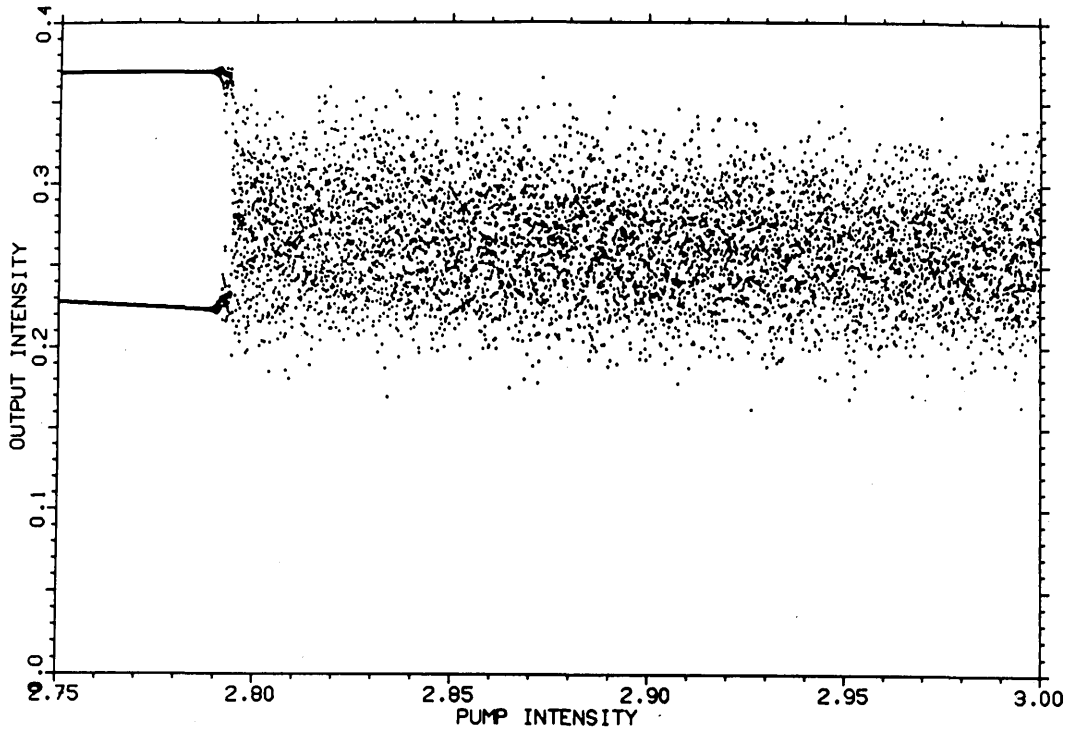

Fig. 20. Bifurcation diagram for a wide-open aperture, representing an example of a modified RTN route to chaos through few bifurcations of an invariant circle.

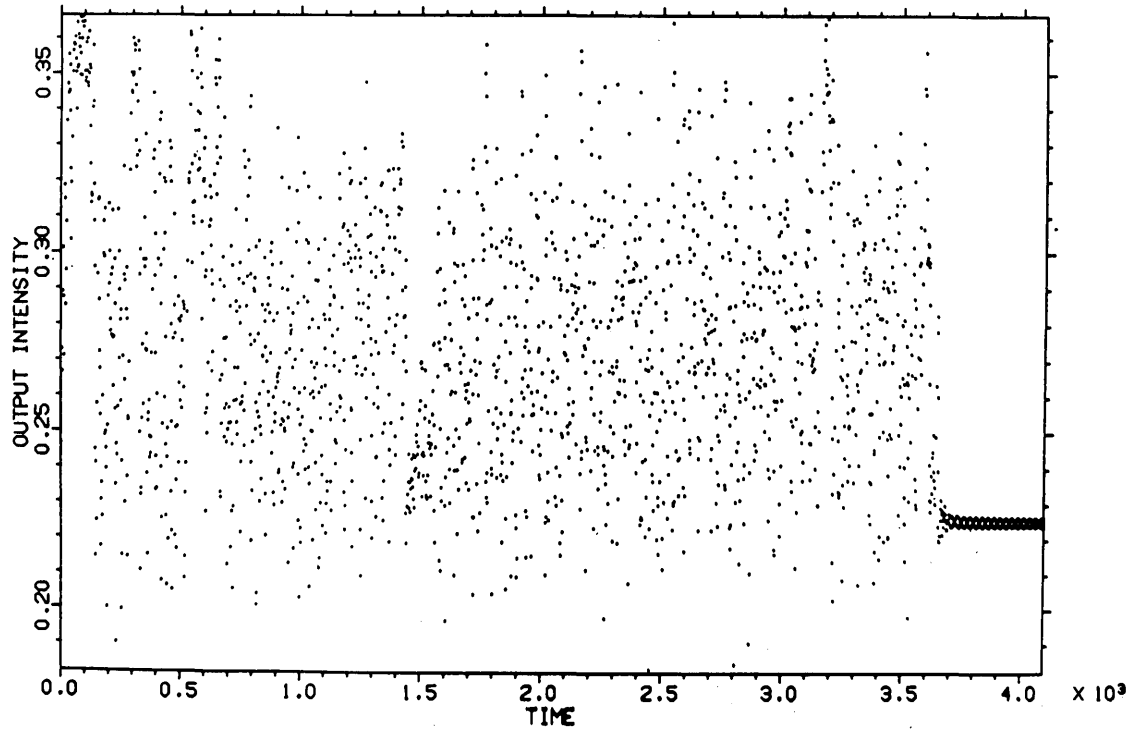

Fig. 21. Time series in the vicinity of the lower period 2 branch from Fig. 20 (I_p = 2.77), with exceedingly long transient chaos. Output intensity of every second round trip is recorded. The period 2 oscillation looks rather like a long-lived wobbling 2 torus. Here, the system is close to a Hopf bifurcation.

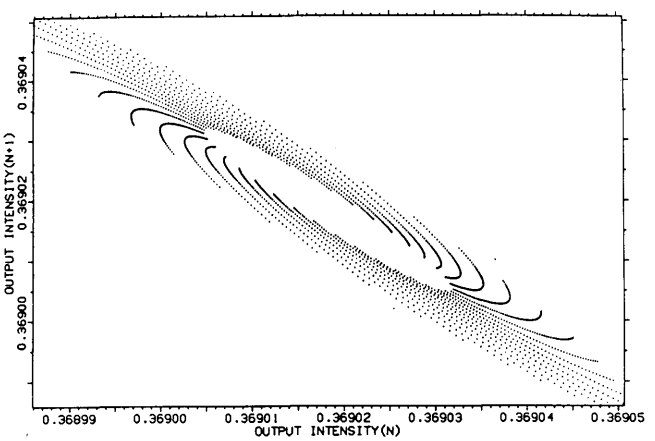

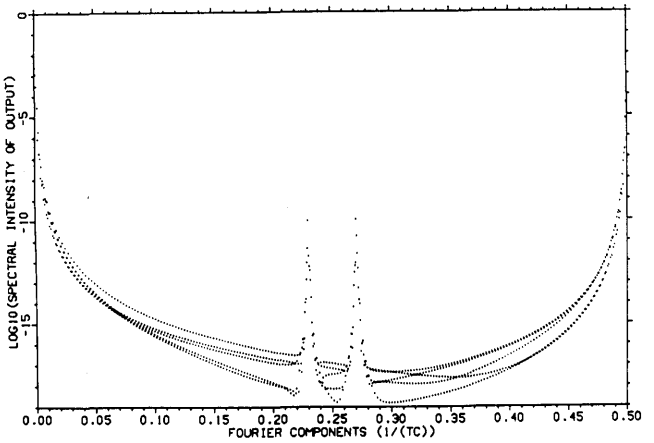

(a)

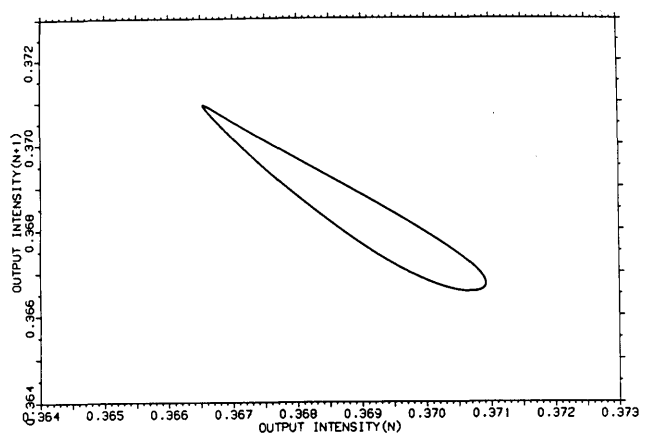

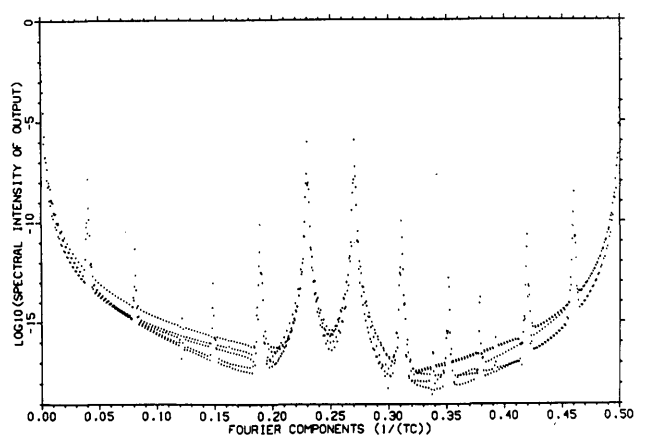

(b)

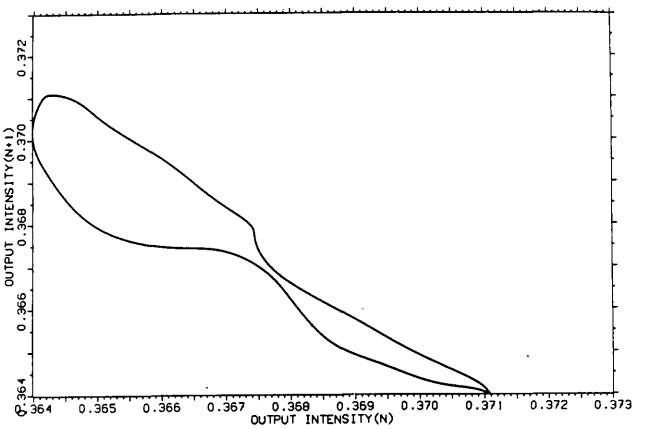

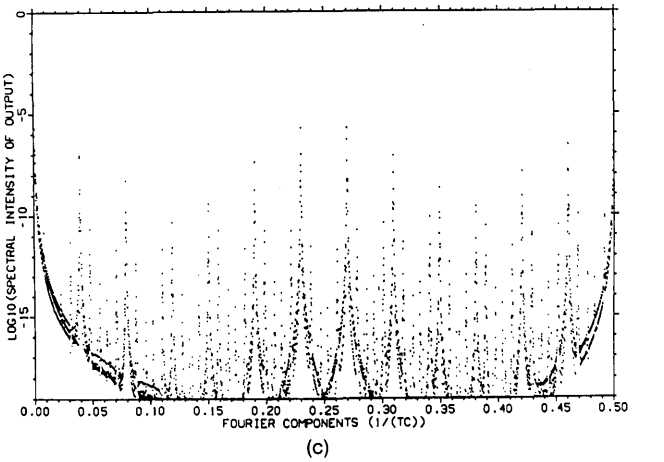

(c)

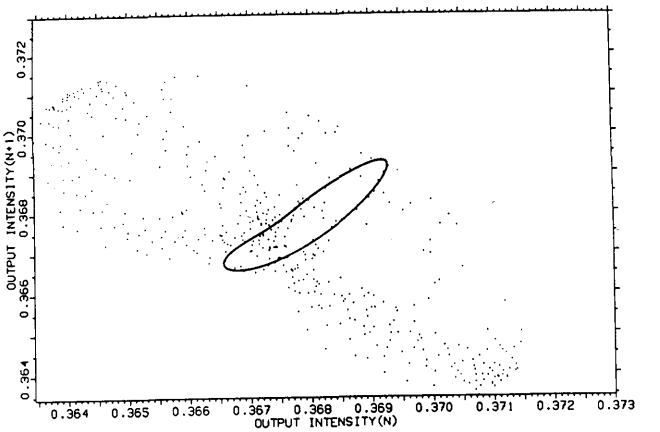

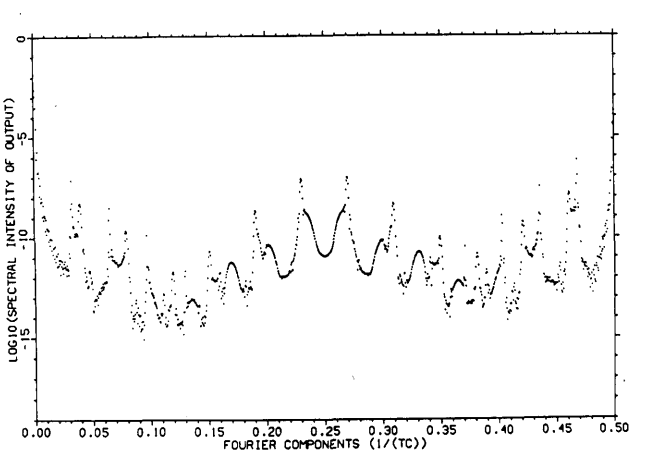

(d)

(*continued overleaf*)

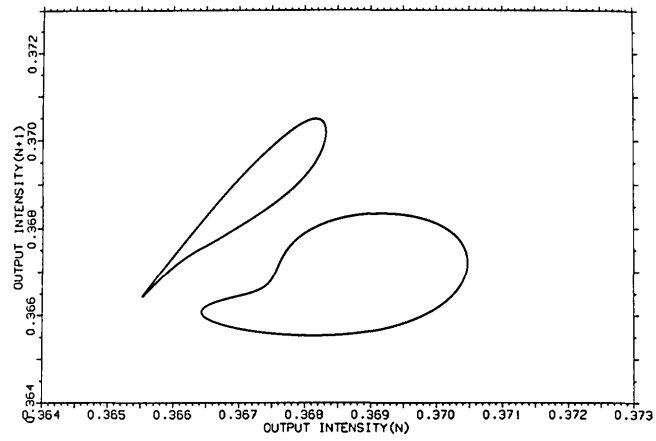
OUTPUT INTENSITY(N+1)
0.364
0.366
0.368
0.370
0.372
0.364 0.365 0.366 0.367 0.368 0.369 0.370 0.371 0.372 0.373
OUTPUT INTENSITY(N)

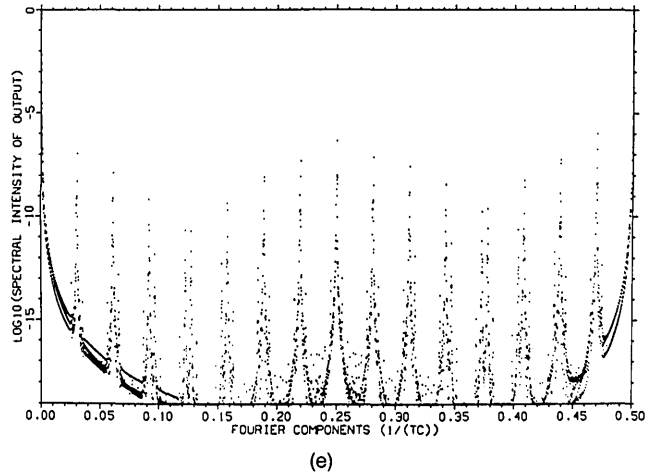
LOG10(SPECTRAL INTENSITY OF OUTPUT)
0
-5
-10
-15
0.00 0.05 0.10 0.15 0.20 0.25 0.30 0.35 0.40 0.45 0.50
FOURIER COMPONENTS (1/(TC))

(e)

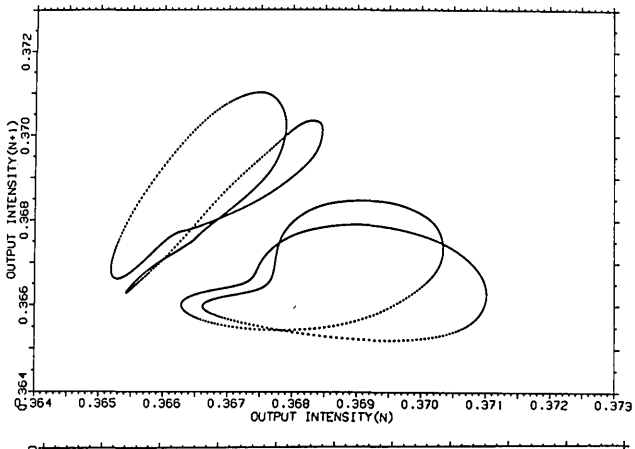
OUTPUT INTENSITY(N+1)
0.364
0.366
0.368
0.370
0.372
0.364 0.365 0.366 0.367 0.368 0.369 0.370 0.371 0.372 0.373
OUTPUT INTENSITY(N)

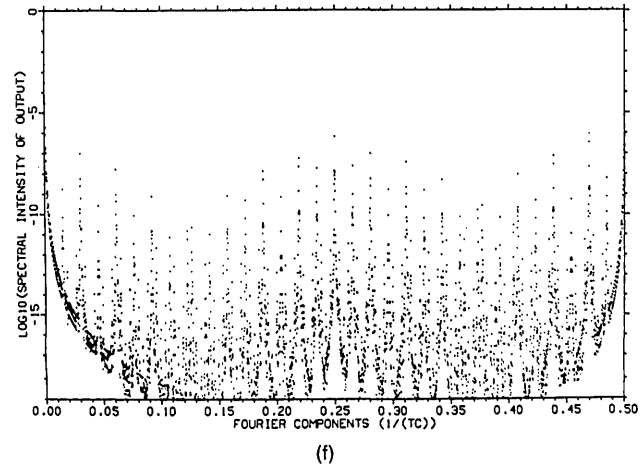
LOG10(SPECTRAL INTENSITY OF OUTPUT)
0
-5
-10
-15
0.00 0.05 0.10 0.15 0.20 0.25 0.30 0.35 0.40 0.45 0.50
FOURIER COMPONENTS (1/(TC))

(f)

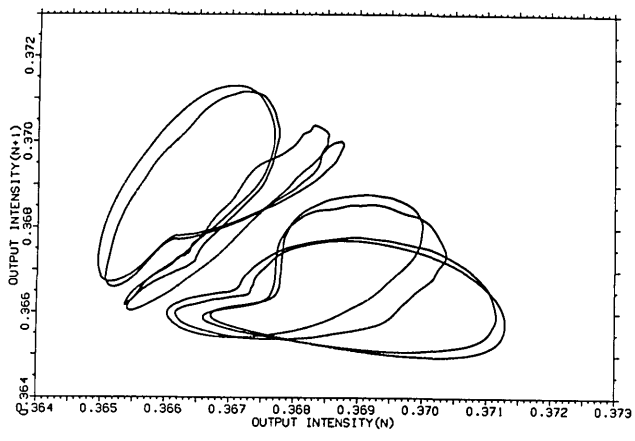
OUTPUT INTENSITY(N+1)
0.364
0.366
0.368
0.370
0.372
0.364 0.365 0.366 0.367 0.368 0.369 0.370 0.371 0.372 0.373
OUTPUT INTENSITY(N)

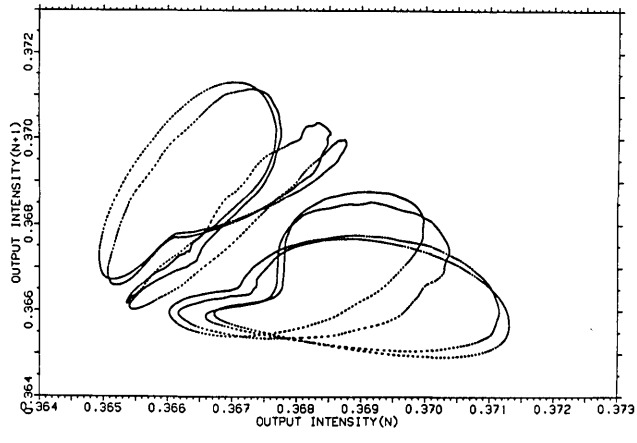
OUTPUT INTENSITY(N+1)
0.364
0.366
0.368
0.370
0.372
0.364 0.365 0.366 0.367 0.368 0.369 0.370 0.371 0.372 0.373
OUTPUT INTENSITY(N)

(g)

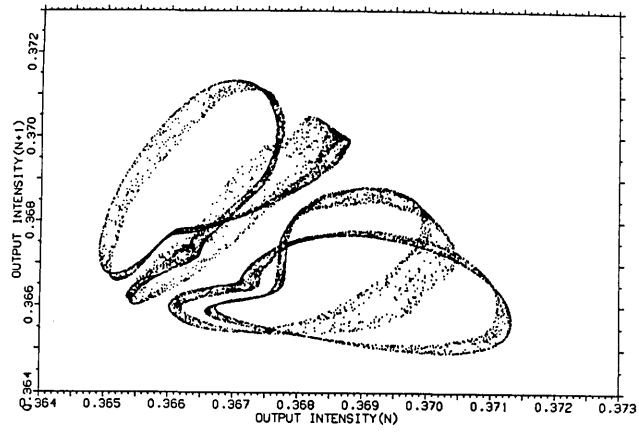
OUTPUT INTENSITY(N+1)
0.364
0.366
0.368
0.370
0.372
0.364 0.365 0.366 0.367 0.368 0.369 0.370 0.371 0.372 0.373
OUTPUT INTENSITY(N)

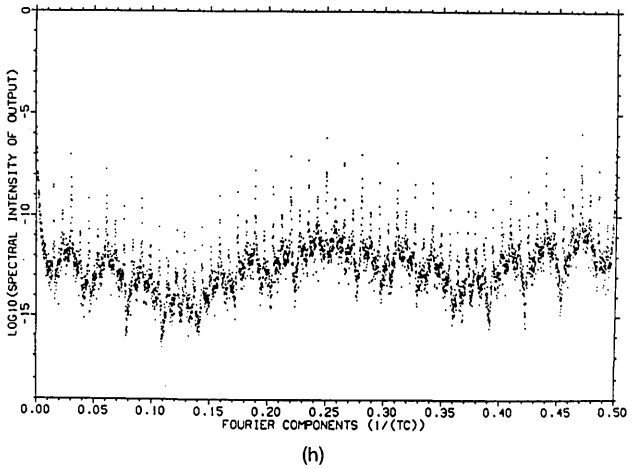
LOG10(SPECTRAL INTENSITY OF OUTPUT)
0
-5
-10
-15
0.00 0.05 0.10 0.15 0.20 0.25 0.30 0.35 0.40 0.45 0.50
FOURIER COMPONENTS (1/(TC))

(h)

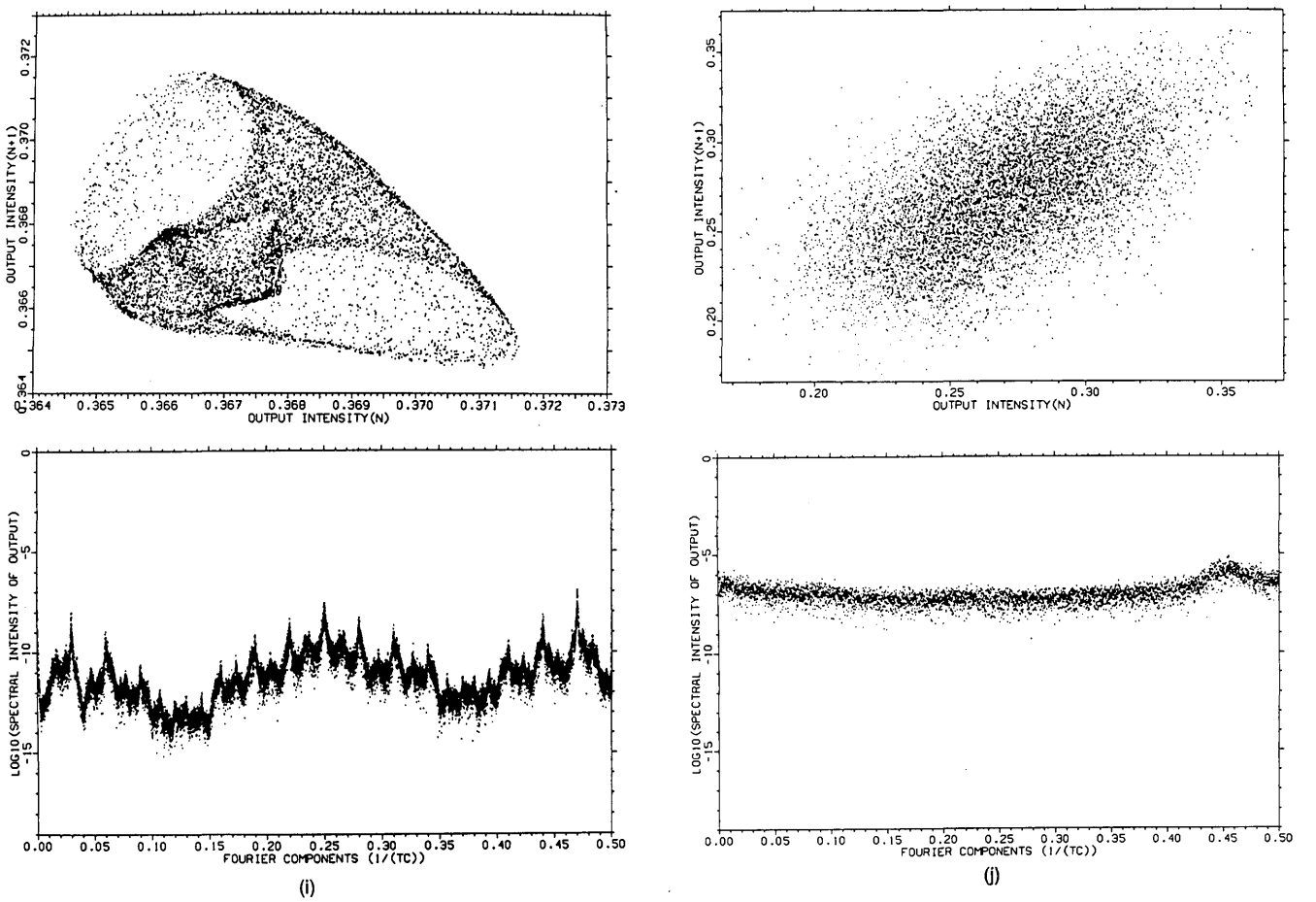

Fig. 22. A series of Poincaré sections and the corresponding spectra for different pump intensities across the transition region from Fig. 20. (a) Spiraling into a fixed point at $I_p = 2.77$. The upper branch of the two period 2 branches from Fig. 20 is shown. Because of the long transient behavior, both $f_1 = 0.5$ and $f_2 \simeq 0.23$ are seen in the spectrum. The third line in the spectrum is the image of f_2 across the 1/4 frequency, a peculiarity of the PCR. The five dotted lines seen in the background of the spectrum are a FFT artifact and have no significance. (b) Well-established limit cycle at $I_p = 2.775$, with many f_2 subharmonics. (c) Developing fractal limit cycle at $I_p = 2.805$, with many subharmonic satellites, ready to explode. (d) Vanishing of the old, and appearance of a new, limit cycle, $I_p = 2.81$. The transient spectrum shows that some lines are receding and that others are growing. (e) First bifurcation of a 2 torus to a 4 torus at $I_p = 2.819$. The spectrum now contains the harmonics of f_1 as well (at 0.25, 0.125, etc.). (f) Further bifurcation at $I_p = 2.8205$. (g) The last bifurcation resolved at $I_p = 2.8216$. At $I_p = 2.82165$ frequency locking is observed: the continuous winding lines start to break into a number of dots. (h) Chaotic bands emerging at $I_p = 2.8217$, with wide broadband chaotic spectrum rising. (i) Further development of chaos at $I_p = 2.8225$. (j) High-dimensional single-branch period 1 chaos at $I_p = 2.825$, with featureless spectrum and nine positive Lyapunov exponents.

the general description and performance of the model are investigated in Refs. 7 and 8; we present and discuss some interesting case studies not reported there.

Little is known about the transition to chaos in infinitely dimensional systems. Farmer[11] has considered the Mackey–Glass time-delay differential equation, and his findings will be used for comparison below. We find that the route to chaos, as the pump intensity is increased, strongly depends on the size of the aperture in front of the normal mirror. For small openings it starts as a Feigenbaum period-doubling single-mode scenario, much like the one-dimensional model from Fig. 2. As the pump intensity gets larger, it gradually acquires the more featureless forms of high-dimensional chaos but occasionally with an interesting periodic window structure. For large-aperture openings, in contrast, it jumps quickly to high-dimensional chaos, usually after only a few bifurcations.

We monitor the transition to chaos by using the different tools at our disposal: bifurcation diagrams, Poincaré sections, Fourier spectra, etc. For an example the spectrum of Lyapunov exponents is calculated, and from it the change in the Lyapunov dimension of attractors is inferred as a function of the pump intensity. Numerically, the procedure differs from the case of a slow medium in that there is no need to iterate a (infinitely dimensional) return map. Thus, for a comparable CPU time (few minutes on a Cray XMP computer), we are able to execute in excess of 10^5 cavity computer), we are able to execute in excess of 10^5 cavity round trips. After each round trip the pump intensity is either slightly increased or left unchanged if we want to look at a time series. The typical increase is of the order 10^{-5}. In this manner we tried to avoid strong dynamical effects and spurious hysteresis behavior[12] in the bifurcation diagrams, as seen in Fig. 12. Our criterion was that the upsweep and the downsweep should coincide. Indeed, this was the case for single-mode or one-dimensional plane-wave analyses, as performed in Fig. 2. However, in some more complicated cases the hysteresis effects persisted and were unaffected by

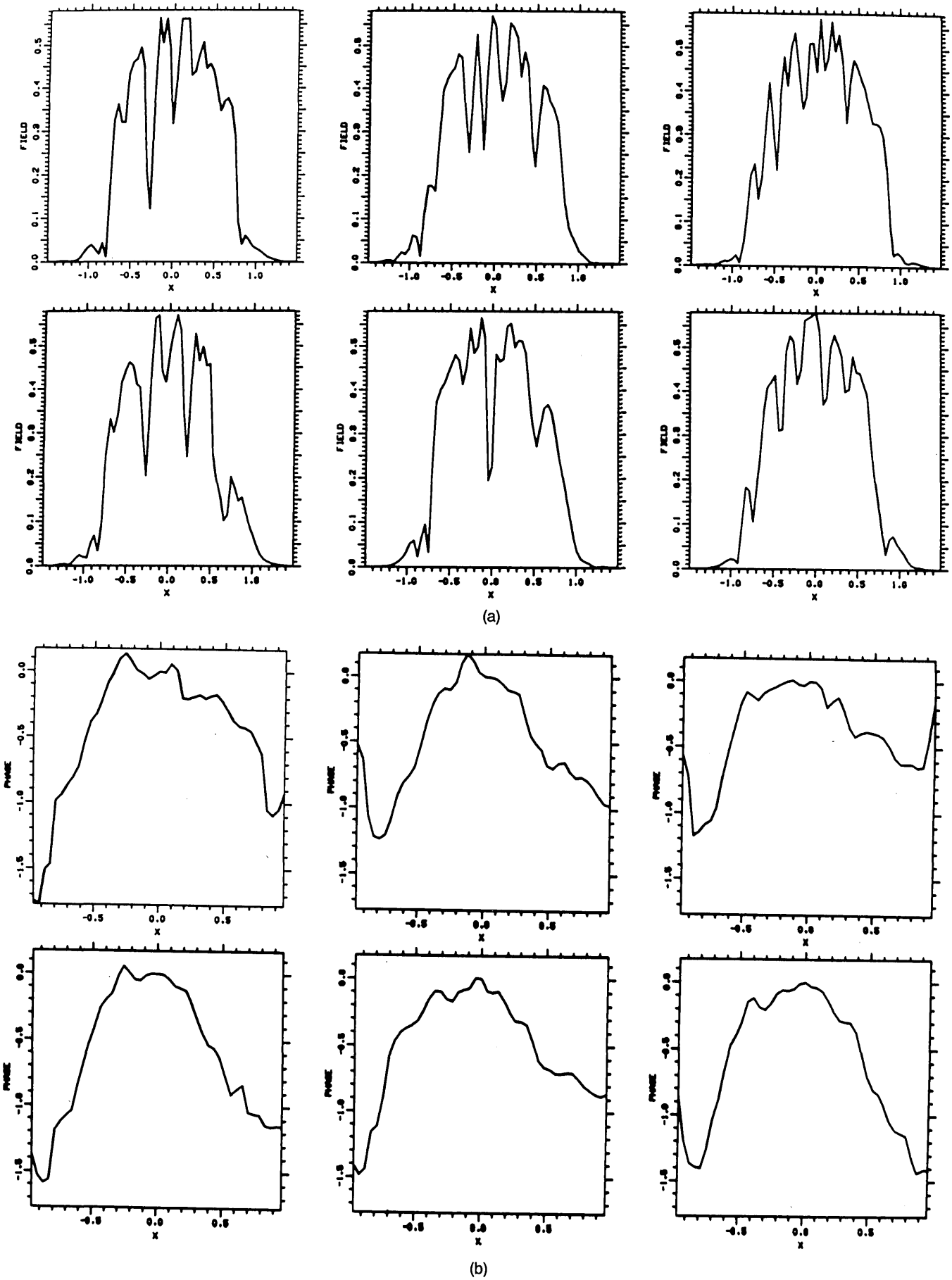

Fig. 23. (a) Transverse profiles and (b) corresponding phase for six consecutive round trips in the fully developed chaos at $I_p = 2.825$.

the slowdown in the sweep rate. In such cases we suspect genuine optical bistability and mode competition to be inherent characteristics of the system.

We start by displaying one such instance in an example already considered in Ref. 8. Its bifurcation diagram is portrayed in Fig. 13. Initially it undergoes Feigenbaum period doublings, which we were able to track down to period-256 oscillations. The small inset in Fig. 13(a) is enlarged in Fig. 13(b), and the small inset in Fig. 13(b) is zoomed and swept up and down in Figs. 13(c) and 13(d). It is seen that the system suddenly jumps from one branch to the other and from one attractor to the other. Such sudden changes in attracting sets, or crises, are common in our system. The sweep slowdown (to 10^{-7}) and plotting of more transient points also resolved more clearly the period-5 window situated in the interval $I_p \simeq 3.44$–3.45. The intermittent chaotic nature of the window is more apparent as the sweep rate is reduced: the window breaks into a number of periodic regions separated by chaotic intervals (Fig. 14). The sweep bifurcation diagrams then look much like the ordinary temporal sequences, as displayed in Fig. 15.

Although it starts as a period 5, the system bifurcates during chaotic bursts (intermittent Feigenbaum), and its spectral content, as depicted in Fig. 16, is not simple. From Fig. 16(b) it is clear that at $I_p = 3.49$ we already have fully developed chaos, since individual spectral lines are gone and a broadband noisy spectrum has risen. This is corroborated further by looking at the spectrum of Lyapunov exponents calculated in Fig. 17 for the intensity interval 3.1–5.0. It is seen that the system becomes chaotic for the first time at $I_p \simeq 3.15$, corresponding to the accumulation point of the first Feigenbaum sequence. At that point the second Lyapunov exponent becomes positive, the first one (describing the indeterminacy of the phase) remaining zero all the time. At approximately $I_p \simeq 3.44$, a large dip in the Lyapunov spectrum occurs, corresponding to our period-5 window. After $I_p \simeq 3.5$, the third Lyapunov exponent becomes positive, after awhile the fourth one, etc., leading to high-dimensional chaos.

The strange attractor that sets in after the last periodic window is captured in Fig. 18. Its Lyapunov dimension D_L increases with the pump intensity and is $D_L \simeq 3.0$ at $I_p = 3.18$ and $D_L \simeq 4.5$ at $I_p = 3.5$. The correlation dimension was also calculated at $I_p = 3.18$, and it amounted to $D_2 \simeq 2.4$ (Fig. 19). Hence the attractor is nonuniformly covered. Also, the rate of increase in the D_L dimension and in the metric entropy decreases with I_p. This is in contrast to the Mackey–Glass delay differential equation, where D_L increases linearly while the entropy is constant.[11] Furthermore, Lyapunov exponents in the Mackey–Glass system converge to zero, and in the PCR they increase monotonically. Thus a chaotic attractor of a given dimension has more unstable directions in the Mackey–Glass system than in the PCR, but these are weakly chaotic in comparison with the fewer, but strongly chaotic, directions of the PCR. A more detailed discussion of the dimension and Lyapunov spectrum of our system is provided in Ref. 8.

The foregoing analysis is performed for a medium aperture size: $u = 1$ in units of the pump beam waist. When the aperture is wide open ($u = 8$ in the example that follows), a completely different scenario emerges. Its bifurcation diagram is depicted in Fig. 20. Any resemblance to Fig. 13 (even less to Fig. 2) is gone. The diagram past the sudden transition at $I_p \simeq 2.8$ is featureless, characteristic of high-dimensional chaos. Loosely speaking, opening of the aperture increases the number of ways (or modes) in which the system can develop, i.e., the size of (the portion of) the phase space available to the system is enlarged. We investigated the transition and found that it represents a case of a RTN route of few bifurcations of a limit cycle, leading directly to the fully developed chaos.

One of the first things noticed was an enormous prolongation of the transient response, as seen in Fig. 21. The system tends to wander for thousands of round trips before settling on an attractor. This necessitated killing of many transients before plotting bifurcation diagrams or Poincaré sections. Nonetheless, such a situation is ideal for investigating the transient chaos and the structure of repellers[13] (which we did not perform). In some figures, however, we deliberately kept the transients in order to emphasize some less salient dynamical features.

The transition to chaos is depicted in a series of figures, collected in Fig. 22. The left-hand column of figures in each set represents a series of Poincaré sections through the attracting regions, and the right-hand column represents the spectral content of the dynamics from the left [except for Fig. 22(g)]. The spectrum is obtained by letting the time

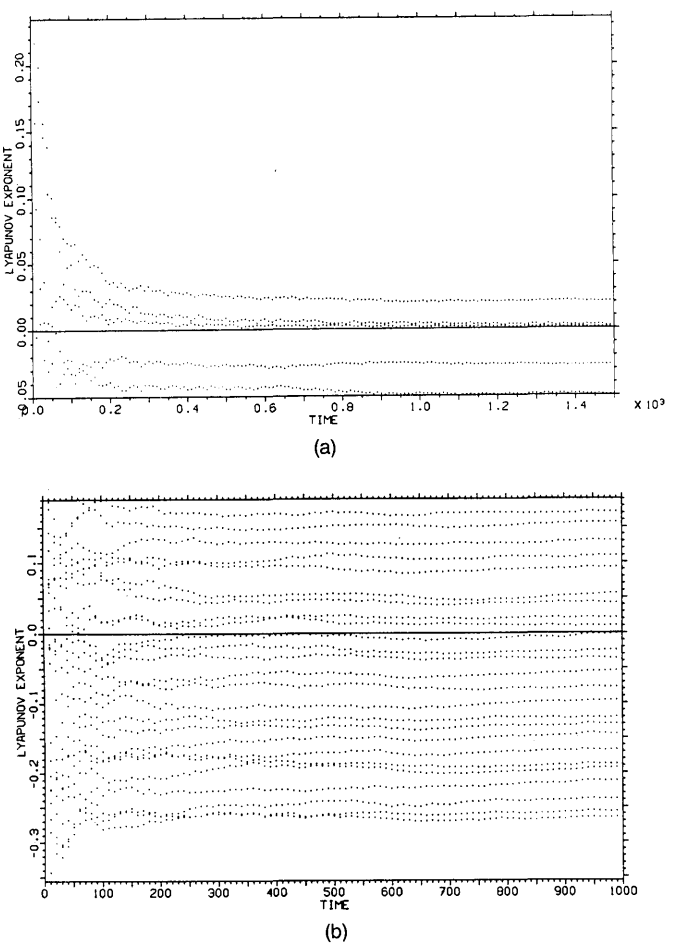

Fig. 24. Temporal development of the spectrum of Lyapunov exponents at the sudden jump from a low-dimensional chaos at $I_p = 2.8225$ in (a) to the high-dimensional RTN chaos at $I_p = 2.825$ in (b).

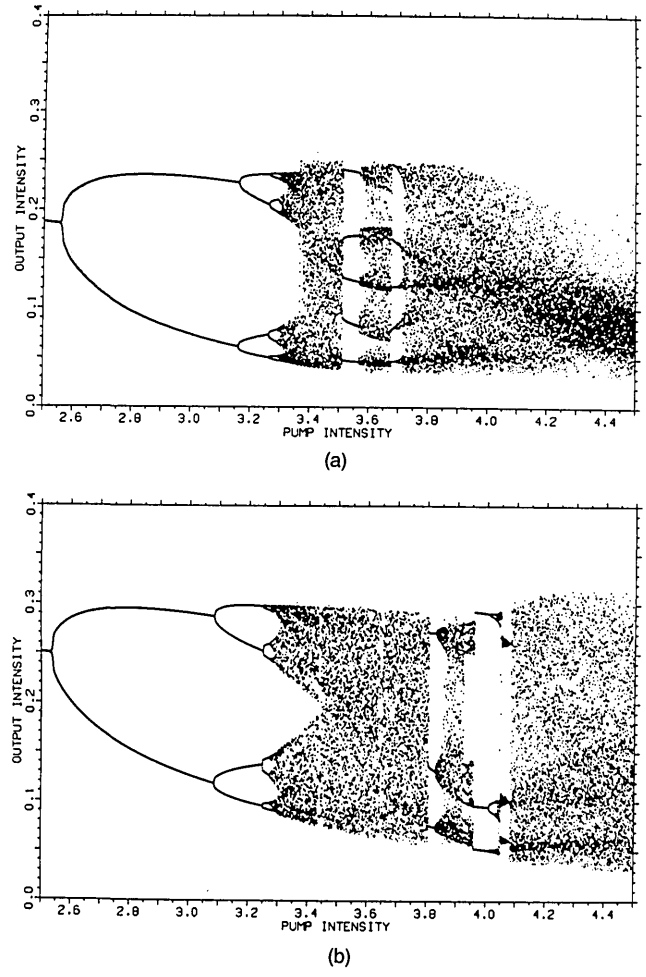

Fig. 25. Bifurcation diagrams for small aperture size, $u = 0.7$, and nearly confocal resonator configuration, $L/R = 0.9$: (a) defocusing medium, (b) focusing medium. Sudden changes of attractors are noted in the windows around $I_p = 4.0$. Around $I_p \simeq 4.1$, in the period 3 window remerging Feigenbaum trees are visible.

sequence $I_{f,n}$ of the forward-integrated intensity after each round trip pass through a FFT analyzer and by squaring the modulus afterward. By using this procedure and by keeping in mind that we are dealing with a PCR, we see that the whole frequency region encompasses only the interval 0–0.5 (in units of the inverse round-trip time).

At $I_p = 2.77$ the system is very close to a Hopf bifurcation. It spirals down to a pair of fixed points corresponding to the simple period-2 half-axial mode [Fig. 22(a)]. However, exceedingly long transients make it appear as a limit cycle, with the second frequency located approximately at 0.23. Taking into account that it spirals along 37 arms, the period amounts to approximately 74 round-trip times. The doublet seen in the spectrum is actually the f_2 and its image across the 1/4 frequency, another peculiarity of the PCR. These frequencies are responsible for the beatings noted in Fig. 21. At $I_p = 2.775$ the limit cycle is well established, and higher-order harmonics of f_2 are already seen as well. At $I_p = 2.805$ it develops a kinky fractal structure, with many harmonics visible in the spectrum, and at 2.81 it explodes, yielding a different attractor [Fig. 22(d)]. The change from a smooth curve to a fractal or a dotted one is an indication of an imminent breakdown of the limit cycle. The new attractor on a downsweep is stable up to $I_p = 2.805$, which is when the old one reappears. Such hysteresis effects, as in the earlier case, indicate that more than one stable state or attractor coexist in the phase space. This new limit cycle contains harmonics of the leading 1/2 mode, and its second frequency is much lower, $f_2 \simeq 0.03$. It readily bifurcates at $I_p = 2.819$, then again at 2.8205, and finally at 2.8216. At $I_p = 2.82165$ a trace of frequency locking is observed and is visible in the pair of Fig. 22(g). Frequency locking is a sign of approaching transition to chaos, which actually happens at $I_p = 2.8217$. In this respect our system is similar to fluid turbulent Rayleigh–Bernard flows with a low aspect ratio.[4,14] In the tiny interval that precedes the transition we were unable to resolve any further bifurcations. At the pump intensity of 2.825 (Fig. 23) we already observe high-dimensional chaos with nine positive Lyapunov exponents [Fig. 24(b)]. Thus opening of the aperture puts at the system's disposal many degrees of freedom or many unstable directions in which to grow.

On the contrary, reducing the aperture size inhibits the system, which has a tendency of developing along Feigenbaum-like one-dimensional scenarios. By even further re-

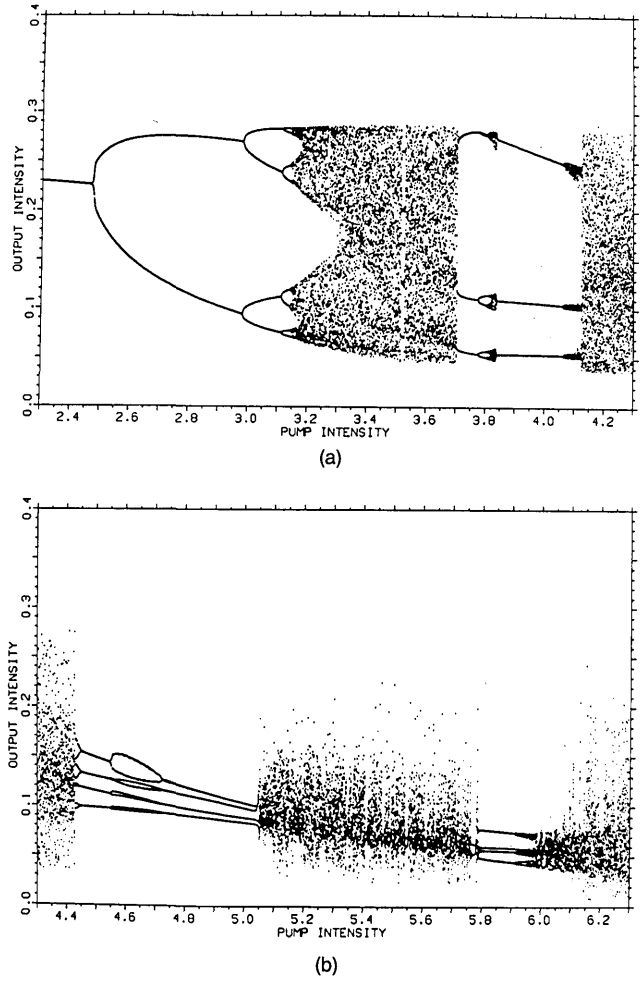

Fig. 26. Same as Fig. 25(b) but with a confocal configuration, $L/R = 1$. The bifurcation diagrams are hardly distinguishable up to the period 3 window. However, in the present case a strange-looking period 4 window opens at $I_p \simeq 4.4$, with primary period bubbles forming at $I_p \simeq 4.6$. (b) A continuation of (a).

duction in the size of the aperture (to values of u less than 1), the system has even less space to develop, and because it is dependent on more than one control parameter, the conditions for appearance of reemerging period bifurcations are met.[15] Indeed, we observe such inverse bifurcations in an infinitely dimensional dynamical system such as ours. They are displayed without comment in Figs. 25 and 26.

4. CONCLUSIONS

In this paper we have investigated routes to optical turbulence in a PCR. It is turbulence and not simply chaos because, in addition to temporal chaos, strong modulations and irregularities are observed in the spatial domain as well. A rich variety of phenomena is observed, making nonlinear-optical resonators, phase conjugate or not,[10] one of the premier physical systems for investigations (numerical or experimental) of the different paths to a turbulent state.

Our results indicate that a reliable and complete description of the dynamics and instabilities in the PCR requires inclusion of the transverse effects. Dynamics that follow from a two-dimensional plane-wave analysis, as exemplified by Fig. 2, and from an infinitely dimensional transverse model, as considered in the rest of the paper, do indeed differ substantially.

In the case of a slow Kerr medium and for a low diffraction geometry, two types of instability occur: slender, strongly diffracting, asymmetric transverse modes in focusing media, and modulational (Benjamin–Feir) spiky, but relatively stable, broader modes in defocusing media. High diffraction offers a larger range of stable solutions (up to $I_p \simeq 7.5$) at the pump frequency. At high enough pump intensity these modes eventually become unstable, breaking the symmetry and at first executing a periodic left–right dance. At still higher intensities the PCR dynamics exhibits an intermittent chaotic behavior with strong hysteresis effects. The detailed understanding of these and other phenomena observed in the transition to chaos in a PCR is rather poor at present, but the results are in general agreement with the trend in other fields of optical instability: The inclusion of transverse effects introduces new instabilities, which can, however, be reduced by the effects of diffraction.

A fast medium, with a faster numerical scheme, permits more comprehensive and detailed probing into the transition dynamics. A variety of possible routes to chaos is observed, as described in Section 3. However, a note of caution is needed in light of the recent results of LeBerre *et al.*[16] They showed that in a passive ring cavity there is no continuous limit between the short but finite medium response time and the instantaneous response time for a plane-wave model. In essence, they note that the routes to chaos are different for a two-dimensional instantaneous and an ∞D time-delay model, what is also found here. The results reported here, however, are for an instantaneous response time (and an ∞D model); however, we have also performed calculations for a short MRT[17] and found that in general they agree when there are no instabilities that are shorter than the MRT in the system. Nonetheless, notable differences persisted in the dynamics; for example, no symmetry breaking of the transverse profile was observed, and the system preferred to go to chaos through a RTN scenario. Considerable mathematical (numerical) difficulties in the treatment of the fast but finite MRT models of a PCR in space and time still preclude definitive comparisons and conclusions, at least for the time being. Clearly, more work and more powerful computers are needed to resolve this and many other dynamical puzzles on the road to a better understanding of optical turbulence.

ACKNOWLEDGMENTS

The part of this work performed in Tucson was supported by the Optical Circuitry Cooperative, and the computations were performed at the National Science Foundation John von Neumann Computer Center in Princeton, New Jersey.

* Present address, Dornier System GmbH, 7990 Friedrichshafen, Federal Republic of Germany.

† Permanent address, Institute of Physics, P. O. Box 57, 11001 Belgrade, Yugoslavia.

REFERENCES

1. As an introduction, see H. G. Schuster, *Deterministic Chaos* (Physik Verlag, Weilheim, 1985).
2. On the linear analysis of modes in a PCR see A. E. Siegman, P. A. Belanger, and A. Hardy, in *Optical Phase Conjugation*, R. A. Fisher, ed. (Academic, New York, 1983), Chap. 13.
3. J. R. Ackerhalt, P. W. Milonni, and M. L. Shih, Phys. Rep. **128,** 205 (1985); R. W. Boyd, M. G. Raymer, and L. M. Narducci, eds., *Optical Instabilities* (Cambridge U. Press, Cambridge, 1986).
4. H. L. Swinney, Physica **7D,** 3 (1983); A. Libchaber, S. Fauve, and C. Laroche, Physica **7D,** 73 (1983).
5. N. B. Abraham, L. A. Lugiato, and L. M. Narducci, J. Opt. Soc. Am. B **2,** 1 (1985).
6. E. M. Wright, P. Meystre, and W. J. Firth, Opt. Commun. **51,** 428 (1984); G. Reiner, P. Meystre, and E. M. Wright, J. Opt. Soc. Am. B **2,** 982 (1985).
7. G. Reiner, P. Meystre, and E. M. Wright, J. Opt. Soc. Am. B **4,** 675 (1987).
8. G. Reiner, P. Meystre, and E. M. Wright, J. Opt. Soc. Am. B **4,** 865 (1987).
9. N. Metropolis, M. L. Stein, and P. R. Stein, J. Combin. Theory **A15,** 25 (1973); H. Bai-Lin, International Center for Theoretical Physics, Trieste (personal communication, 1987).
10. J. V. Moloney, Phys. Rev. A **33,** 4061 (1986); D. W. McLaughlin, J. V. Moloney, and A. C. Newell, Phys. Rev. Lett. **51,** 75 (1983).
11. J. D. Farmer, Physica **4D,** 366 (1982).
12. R. Kapral and P. Mandel, Phys. Rev. A **32,** 1076 (1985).
13. H. Kantz and P. Grassberger, Physica **17D,** 75 (1985).
14. J. P. Gollub and S. V. Benson, in *Pattern Formation and Pattern Recognition*, H. Haken, ed. (Springer-Verlag, Heidelberg, 1979).
15. M. Bier and T. C. Bountis, Phys. Lett. **104A,** 239 (1984).
16. M. LeBerre, E. Ressayre, A. Tallet, and H. M. Gibbs, Phys. Rev. Lett. **56,** 274 (1986).
17. G. Reiner, Ph.D. dissertation (Ludwig-Maximilians-Universität, München, 1987).

(*see overleaf*)

M. R. Belić

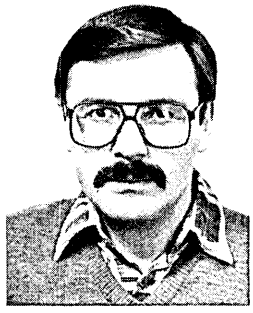

M. R. Belić was born in 1951 in Yugoslavia. He received the B.Sc. degree in physics from the University of Belgrade, Yugoslavia, in 1974, and the Ph.D. degree in physics from the City College of New York in 1980. He spent 1980 and 1981 as a research associate at the Optical Sciences Center, University of Arizona, Tucson, Arizona, and from 1986 to 1987 as a Humboldt Fellow at the Max-Planck-Institut für Quantenoptik, Munich, Federal Republic of Germany. He is now an associate professor at the Institute of Physics, Belgrade, Yugoslavia. His current research interests include phase conjugation, instabilities, chaos in optical systems, and solitons—in general, nonlinear optics and nonlinear dynamics.